ELSEVIER

Polymer 42 (2001) 1055–1065

polymer

www.elsevier.nl/locate/polymer

Two-phase nanoscale morphology of polymer/LC composites

R.A. Vaia[1], D.W. Tomlin, M.D. Schulte, T.J. Bunning*

Air Force Research Laboratory, Materials and Manufacturing Directorate, AFRL/MLPJ and AFRL/MLBP, 3005 P. St., Bldg 651, WPAFB, OH 45433-7702, USA

Received 10 April 2000; received in revised form 1 June 2000; accepted 12 June 2000

Abstract

Small-angle X-ray scattering and high-resolution scanning electron microscopy (SAXS/HRSEM) were utilized to examine the nano (1–100 nm) and meso (100–1000 nm) scale morphology of polymer dispersed liquid crystal (PDLC) films of varying liquid crystal (LC) concentration. In contrast to the conventional PDLCs derived from photo-initiated step-growth polymerizations, these PDLC films were formed using photo-irradiation of initially homogeneous syrup comprised of highly functional free-radical monomer and liquid crystal, resulting in rapid molecular weight increase and network formation prior to or in conjunction with phase separation. Two-phase morphology observable with HRSEM was absent below 20% LC, although fine, small modulation features existed on the fracture surface. In contrast, SAXS reveals increasing nanoscale heterogeneity with increasing LC content. The scattering behavior is consistent with a structure factor derived from an Ornstein–Zernicke model indicating that composition fluctuations frozen by network formation exist at the lowest LC concentrations. At higher LC concentrations, a discontinuous LC phase is observed which coalesce into a co-continuous polymer/LC phase between 35 and 40% LC. Above this regime, aggregated beads of polymer form whose size and uniformity steadily increase with concentration. These morphological observations are consistent with analysis of the SAXS data via a two component Debye–Bueche model at low q. The nanoscale features of the PDLCs formed from highly functional free-radical monomers underscore the importance of the polymerization mechanism in controlling the two-phase morphology in PDLCs. © 2000 Published by Elsevier Science Ltd.

Keywords: Polymer dispersed liquid crystal; Polymerization-induced phase separation; Small angle X-ray scattering

1. Introduction

Polymer dispersed liquid crystals (PDLCs) are of technological importance in the development of switchable windows, electro-optic shutters, displays, and most recently switchable gratings [1,2]. The most versatile method to form PDLC structures is photo-initiated polymerization of an initially homogenous mixture containing reactive monomers and liquid crystal molecules. These pre-polymer syrups are typically solvent free and have low viscosity. Large variations in the final two-phase structure can be obtained by varying either the LC composition, the intensity of the curing radiation, or the photo-polymerization chemistry (free-radical or step-growth). The breadth of accessible two-phase structure results in a broad range of electro-optical properties.

Although the final structure/property relationships for PDLCs has been examined extensively, most of the emphasis has been with respect to the relationship between inherent LC properties (elastic constants, viscosity, dielectric anisotropy, birefringence) and the electro-optical properties of the two-phase structure (contrast ratio, switching speeds). However, the optical characteristics of the PDLC film are also dependent on the details of the polymer structure and thus the nature and rate of polymerization mechanism and the role of small molecule additives. Understanding and controlling the polymerization mechanism is especially important for holographic curing of PDLC films (H-PDLC), in which a spatial variation of light intensity results in a patterned LC droplet distribution [3–5]. The spatially varying differences of the two-phase structure are key in determining the performance of these switchable diffractive structures (transmissive or reflective).

Recent HPDLC developments by our group [6,7] using a free-radical polymerization of highly functional monomers have demonstrated the ability to sequester nanoscale LC domains (<100 nm), thereby eliminating scattering problems associated with larger two-phase structures resulting from step-growth polymerizations. For free-radical reactions, a high molecular weight polymer is formed almost instantaneously, while for a step-growth reaction,

* Corresponding author. Tel: +1-937-255-3808; fax: +1-937-255-1128.
E-mail addresses: timothy.bunning@afrl.af.mil (T.J. Bunning), richard.vaia@afrl.af.mil (R.A. Vaia).
[1] Corresponding author. Tel: +1-937-255-9184; fax: +1-937-255-9157.

0032-3861/01/$ - see front matter © 2000 Published by Elsevier Science Ltd.
PII: S0032-3861(00)00462-6

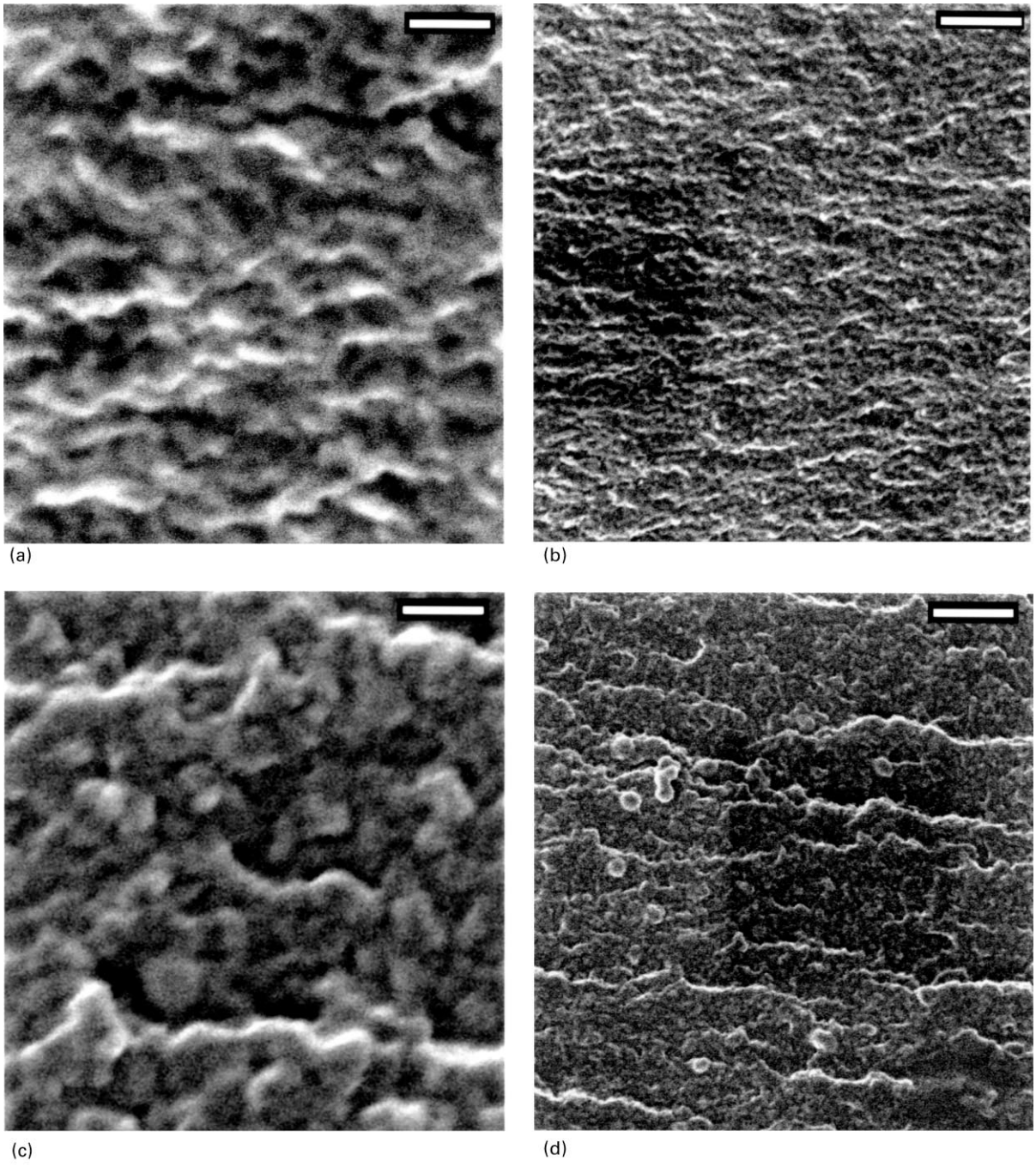

Fig. 1. HRSEM micrographs of 10% (a and b) and 15% (c and d) samples. Scale bars correspond to: (a) 150 nm; (b) 600 nm; (c) 150 nm; (d) 600 nm.

the molecular weight increases slowly with time [8]. In the former case, high molecular weight polymer initially phase separates from the LC-rich polymerizing mixture. The resulting particles are surface rich with functional groups and rapidly aggregate together to form a macroscopic gel. Thus morphology development occurs within an elastic gel. In contrast, for a step-growth reaction, monomer is converted to oligomer early in the reaction but little high molecular weight material exists until the reaction is almost complete. As a consequence, phase separation kinetics and associated time-temperature-transformation (TTT) space are radically different, even though the initial (monomer and LC) and final (polymer and LC) phase diagrams are similar. Thus, the nature of the polymerization mechanism (in addition to LC composition) controls the type of two-phase structure.

In addition to the fundamental aspects of the photo-induced phase-separation (PIPS) process, practical issues associated with the characterization of the nanoscale structure occur. Even though a two-phase structure exists, the

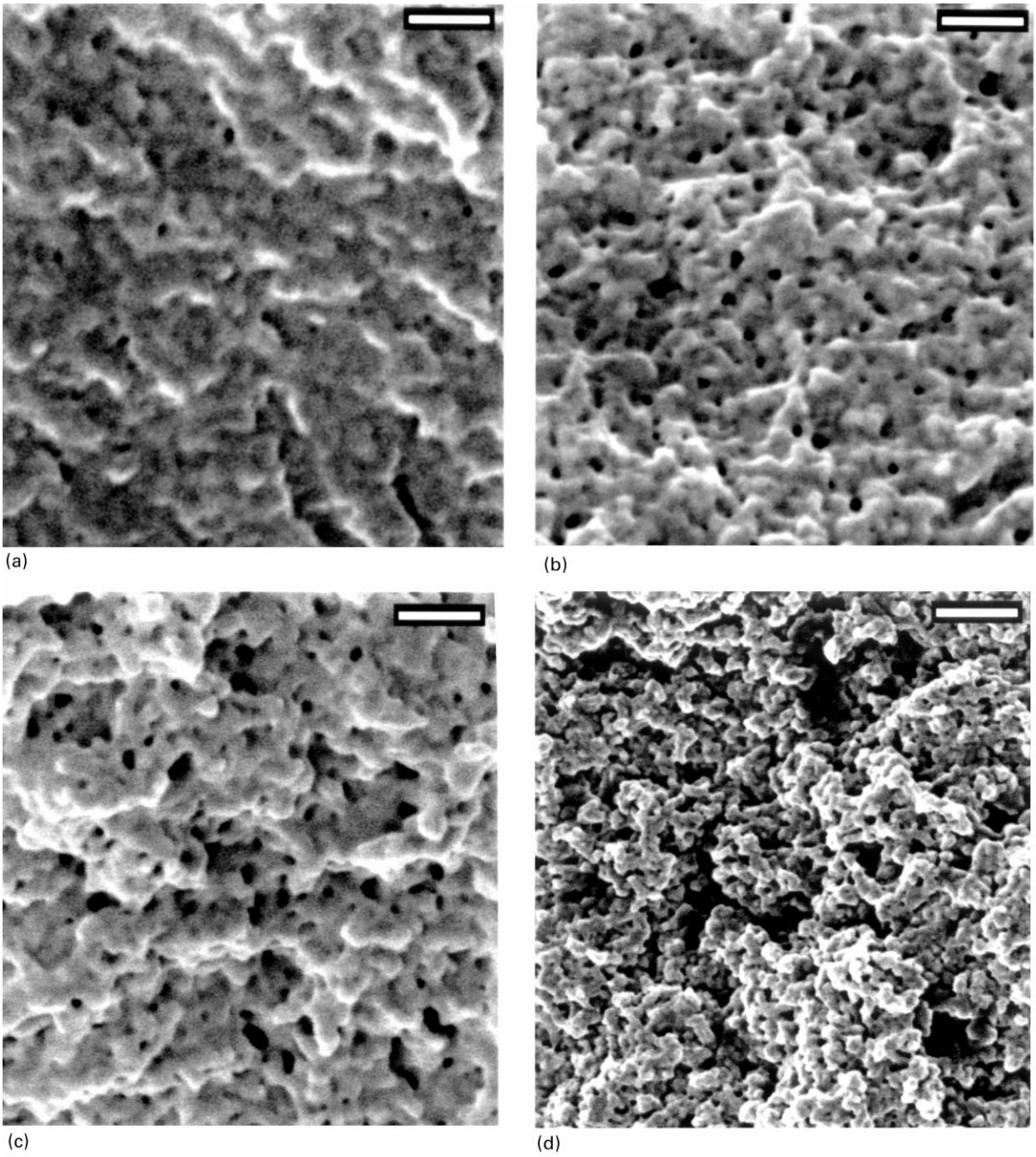

Fig. 2. HRSEM micrographs of: (a) 20%; (b) 28%; (c) 35%; (d) 40%; (e) 45%; (f) 50% LC samples. Scale bars correspond to 150 nm for a–c and 300 nm for d–f.

films are optically transparent due to the nanoscale LC domains. Conventional cloud-point and light scattering techniques are of limited utility. High-resolution electron microscopy of the final morphology has been the preferred method of characterizing these structures [9]. However, since morphology controls the electro-optic properties, enhanced control of domain size, distribution and morphology, whether by processing techniques or additives, is paramount to optimizing performance. This requires the ability to monitor morphology formation in real-time.

This work examines the resultant morphology of photo-initiated phase separation of a penta-acrylate/liquid crystal system. The structural heterogeneity observed with increasing liquid crystal concentration underscores the importance of the polymerization mechanism in controlling the two-phase morphology in PDLCs. The nano (1–100 nm) and meso (100–1000 nm) morphology is characterized using complementary information from small-angle X-ray scattering (SAXS) and high-resolution scanning electron microscopy (HRSEM). A comparison of the pertinent length

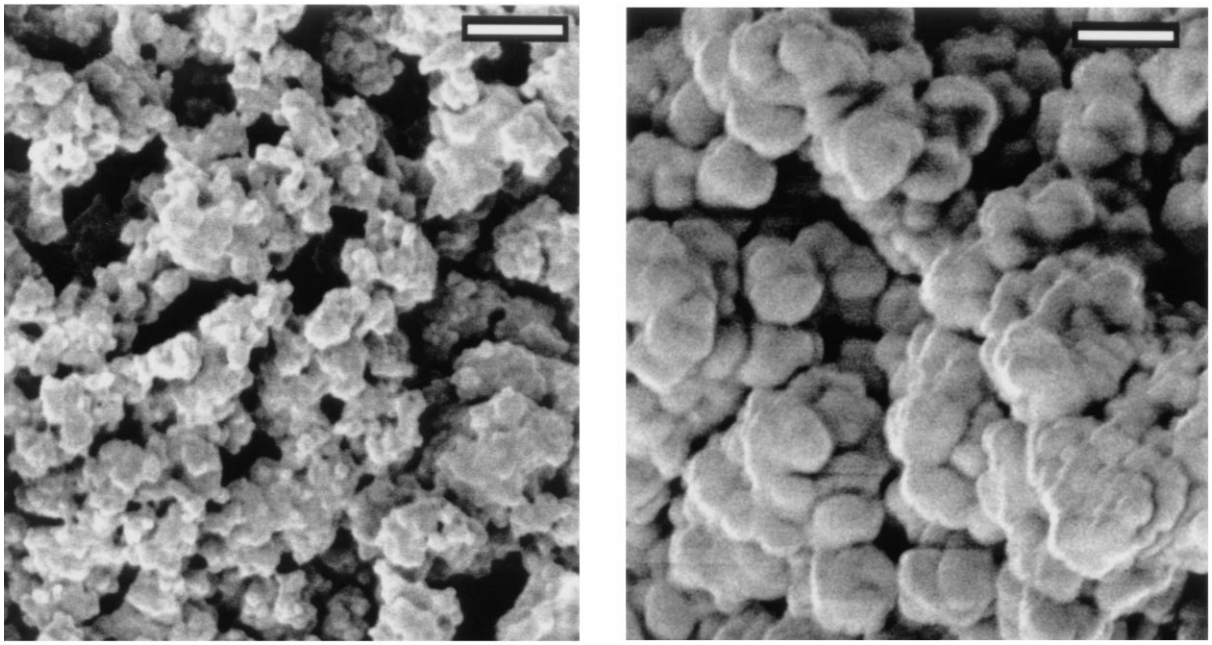

Fig. 2. (*continued*)

scales obtained by each technique suggests performing dynamic studies would be beneficial.

2. Experimental

2.1. Materials

Pre-polymer syrups consisted of a penta-acrylate monomer (81.25%), photoinitiator rose bengal (0.25%), co-initiator *n*-phenyl glycine (NPG-2.0%), and homogenizer *n*-vinylpyrrolidinone (16%). All compounds were obtained from Aldrich except rose bengal, which was obtained from Spectra Group. This isotropic syrup was thoroughly mixed with the liquid crystal E7 (EM Industries), leading to systems containing 0–50% E7. All percentages refer to weight %. Films 1 mm thick were exposed to two 20 W halogen lamps (one each side) for approximately 20 min. The incident power on the samples was approximately 120 mW/cm^2.

2.2. Characterization

Low-voltage, high-resolution scanning electron microscopy (SEM) was employed for morphological studies using a Hitachi S-900 scanning electron microscope with a 1 keV accelerating voltage and the images captured using Quartz PCI (Quartz Imaging Corporation). Sample films were prepared for SEM analysis by first peeling them from the glass substrate with a razor blade. The liquid crystal was then extracted over a 12-h period by immersing the free films in methanol. Dried films were mounted on metallic sample stubs with silver paint and then fractured in liquid nitrogen to yield an interface that was representative of the bulk morphology. A 2–4 nm thick coating of tungsten was deposited using a dual ion beam sputter coating apparatus to minimize artifacts associated with sample charging. Note that no difference between the interior and surface morphology was observed.

Small-angle X-ray scattering was performed at the Advanced Polymers Beamline (X27C) of the National Synchrotron Light Source (NSLS), Brookhaven National Laboratory (BNL). The synchrotron X-rays ($\lambda =$ 0.1307 nm, defined by a double multi-layer monochromator) were collimated to a 600 μm beam size using a three pinhole collimator. Data was collected using a Braun linear position sensitive detector [10] at 1942 mm. The scattering angle was calibrated using silver behenate. Absolute calibration of the scattering intensity was not performed so only relative changes in invariant and intensity is meaningful. Data acquisition times were typically 4 min. The raw data was corrected for beam fluctuations and sample absorption. Background scatter was removed via a point-by-point subtraction, weighted by sample transmission, of empty-cell scatter.

3. Results

The concentration of LC impacts a broad range of morphological features, ranging from size, shape and concentration of polymer and LC domains to variations in surface fracture. A progression of the final two-phase

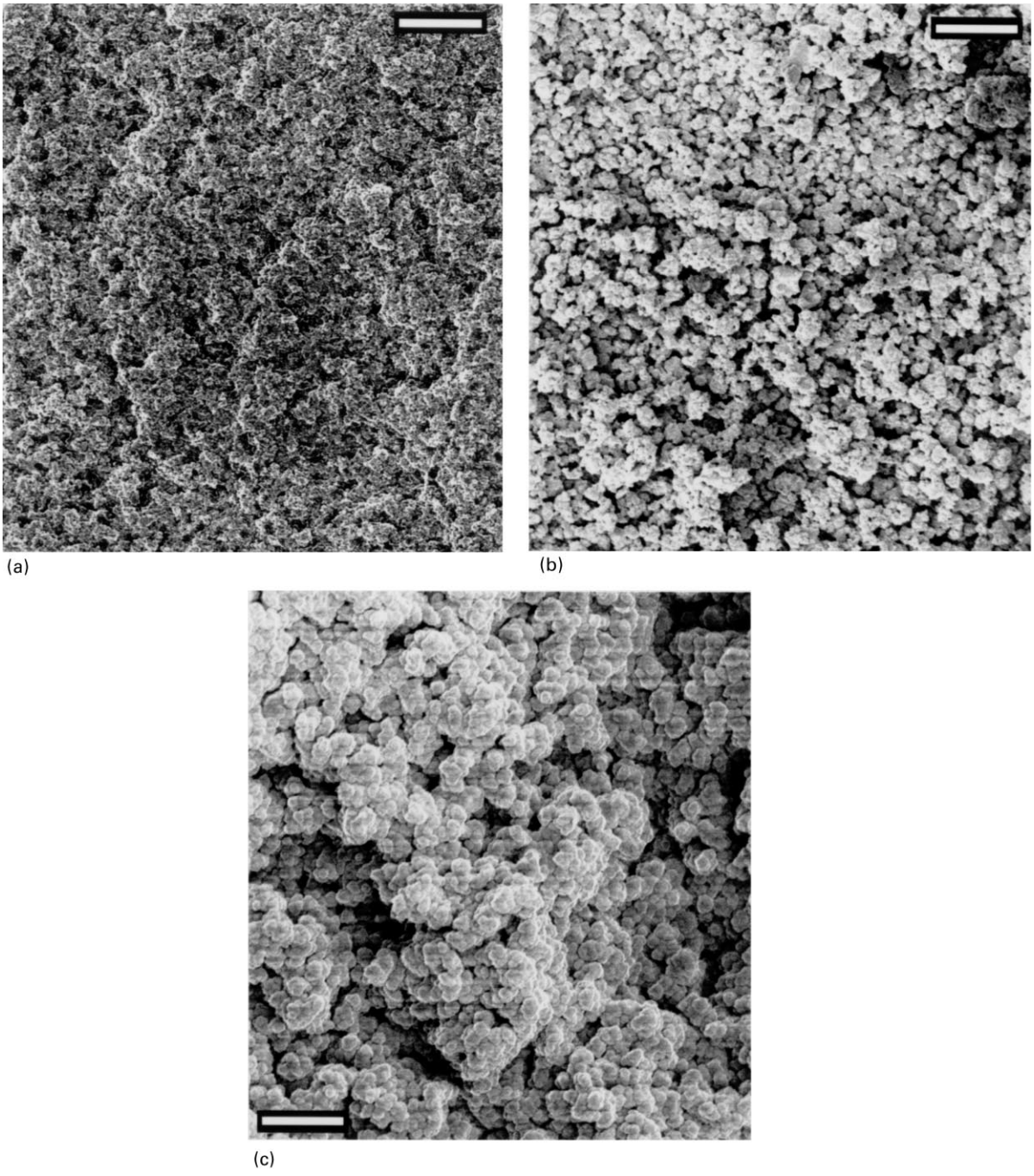

Fig. 3. HRSEM micrographs of: (a) 40%; (b) 45%; (c) 50% LC samples. Scale bar corresponds to 1.5 μ.

structure with LC concentration is summarized in Figs. 1–3. Note that the LC was removed before microscopy, so the dark areas in the micrographs, revealing the absence of material, are representative of the original LC domains.

At concentrations below 20% LC, no discrete domains are observed (Fig. 1). Pure penta-acrylate resin (0% LC) exhibits classical glassy fracture with no resolvable structure on the fracture surface. Localized topography, observed as a textured fracture surface exists with increased LC content (10 and 15% LC, Fig. 1). Both high- and low-magnification pictures reveal a very fine level of texture (10–40 nm) that is attributed to localized differences in the polymer structure.

At 20%, a few small dark areas attributed to voids formed via LC phase separation can be seen (Fig. 2a) and range between 10 and 20 nm. At this high magnification, the considerable surface roughness that was observed of the 20% sample is not typical of a smooth glassy polymer fracture. As the LC concentration increases, the density and size of domains increase, becoming appreciable at LC

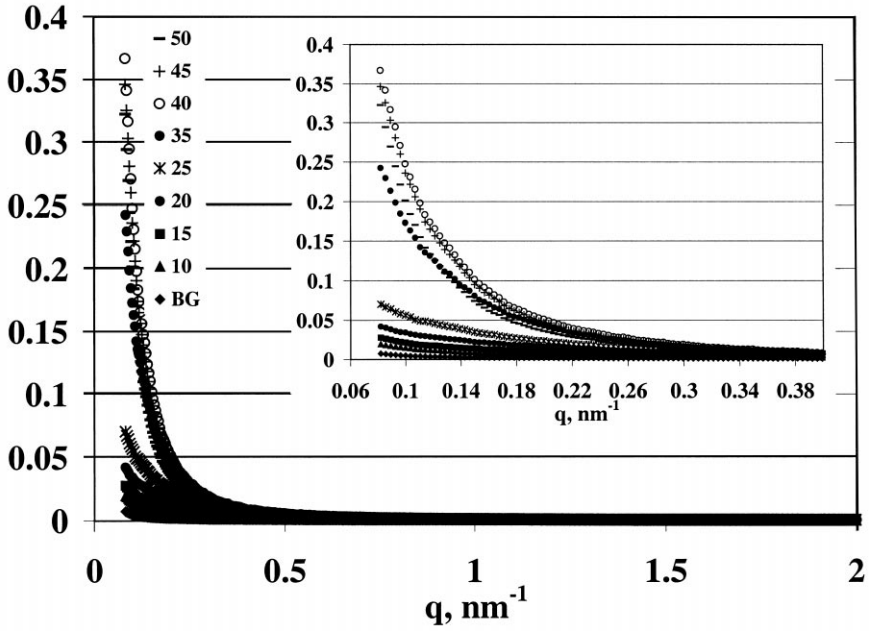

Fig. 4. Raw SAXS data obtained for all LC compositions. Inset shows low q scattering ($0.08\ nm^{-1} < q < 0.4\ nm^{-1}$).

concentrations greater than 25%. For the 28% LC sample (Fig. 2b) the largest domain is approximately 30 nm in diameter, and for the 35% sample (Fig. 2c) it is approximately 50 nm in diameter. For all three cases, the majority of domains are 20–30 nm in size, indicating one phase separation event yielding an increased spatial density with increasing LC concentration and no domain coalescence. The volume fraction of LC domains steadily increases and is estimated to reach 10–15% in the 35% LC sample. Thus, a considerable amount of the LC still resides in the cross-linked matrix. It is interesting to note that because the domain sizes are substantially less than 100–200 nm, macroscopic samples up to 30% LC are optically clear and difficult to distinguish from a 0% sample, even though they exhibit a classic two-phase structure in the micrographs.

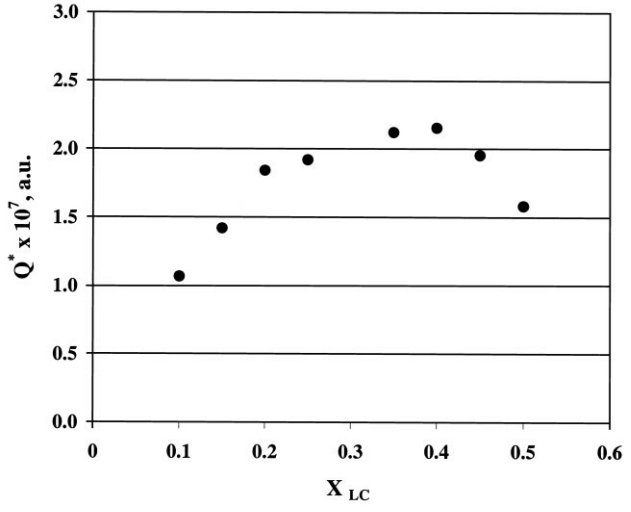

Fig. 5. The partial invariant, Q^*, calculated from the integral between finite limits ($0.08\ nm^{-1} < q < 2.0\ nm^{-1}$) for each LC composition.

At LC concentrations greater than 35% (Fig. 2d–f), the LC phase becomes continuous. Small polymer beads that have aggregated wind through the LC phase creating a co-continuous two-phase morphology. The size of the polymer beads steadily increases with LC concentration, from 75 to 125 nm (40% LC, Fig. 2d) to 250–350 nm (50% LC, Fig. 2f). Concomitantly, the volume occupied by the phase separated LC regions also increases with LC concentration. A more global perspective of the morphology of the 40–50% LC samples is shown at lower magnification in Fig. 3. Individual large pockets of LC exist in the 40% sample. As the LC composition increased, smoother beads and increased LC volume fraction are observed.

Fig. 4 shows the corresponding raw SAXS data for samples examined in the previous micrographs. The scattering curves are essentially featureless with a strong increase in intensity at the lowest scattering vectors, q. The insert shows this upturn more clearly. The presence of finite scattering for the 10, 15, and 20% LC samples indicates that there are morphological differences that are not clearly distinguishable by HRSEM. Note that no appreciable scattering was observed for the unpolymerized syrups, irrespective of LC concentration, or the pure photopolymerized penta-acrylate resin (0% LC). Although the unpolymerized syrups are composed of a mixture of monomers, chain extenders, photoinitiators and LC, no discernable compositional fluctuations, which would manifest in fluctuations of scattering length density, are observable.

To quantify the extent of heterogeneity (scattering density fluctuations) in more detail, the partial invariant,

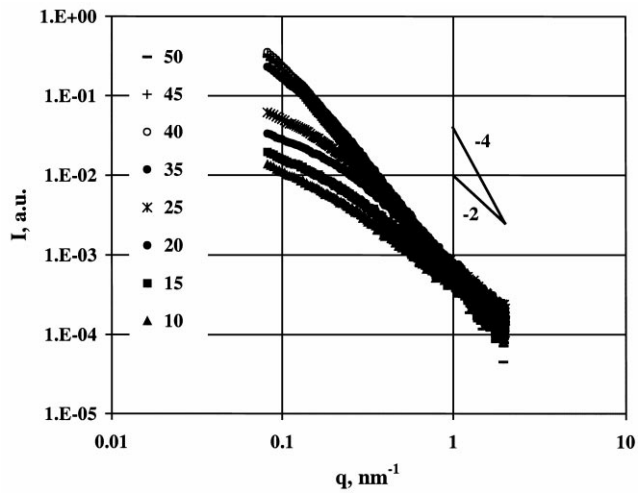

Fig. 6. Intensity versus q for all compositions plotted logarithmically. Lines to guide the eye to slopes of -4 and -2 are shown.

Q^*, was determined from the background corrected scattering data. Recall, the invariant, Q, may be defined [11] and determined directly from the experimental data, $I(q)$, as Eq. (1):

$$Q = \int_0^\infty q^2 I(q)\, \mathrm{d}q \propto \phi_1\phi_2(\rho_1 - \rho_2)^2 \tag{1}$$

where ϕ and ρ are the volume fraction and electron density of the constituent phases. The invariant is independent of structural features, such as shape of particles, which result in significant changes in the shape of $I(q)$. Obtaining data over all scattering vectors ($0 < q < \infty$) is experimentally unfeasible and thus only a partial invariant, Q^*, can be determined directly from experimental data. The integral limits corresponded to $0.08\ \mathrm{nm}^{-1} < q < 2.0\ \mathrm{nm}^{-1}$ where the lower and upper limits are determined by the beam stop and sufficient signal-to-noise, respectively.

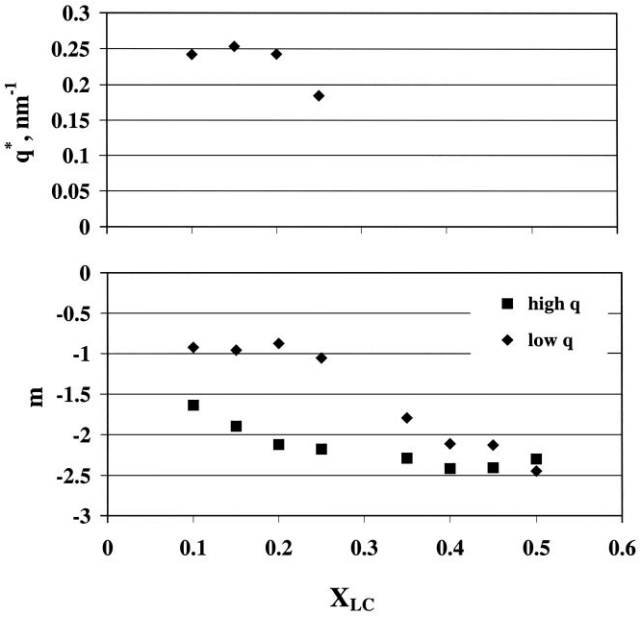

Fig. 7. The critical scattering vector where crossover occurred (top section) and slopes obtained from power-law scaling for both the high q ($0.4 - 2\ \mathrm{nm}^{-1}$) and low q ($0.08 - 0.15\ \mathrm{nm}^{-1}$) regions (bottom section).

Fig. 5 shows the partial invariant determined from background corrected SAXS data for the various concentrations of LC in the pre-polymer syrup. The invariant rises between 10 and 40% LC before decreasing. The maximum occurs approximately at the same composition in which the HRSEM micrographs indicate an inversion in morphology from a continuous polymer matrix with discrete, nanoscale sized LC domains to a semi-continuous LC fluid with aggregated polymer beads. Since the relative fraction of LC in the polymer phase is unknown, the actual volume fraction and contrast of the scattering species is unknown. Nevertheless, the largest degree of nanoscale heterogeneity occurs around $X_{LC} = 0.40$.

Fig. 6 shows the background corrected intensity plotted on a logarithmic scale to emphasize the changes of intensity with scattering vector. Two types of behavior are observed. For LC concentrations 25% and less, the scattering data exhibit two regimes, high and low q, that can be distinguished with different power-law dependencies. In contrast for the highest LC concentrations, essentially uniform power-law behavior is observed over the entire scattering range. Furthermore, a steady rise in the intensity occurs as LC concentration is increased from 10 to 25% while minimal change in magnitude occurs from 35 to 50%.

Power-law scaling of scattering intensity and associated fractal analysis of the exponents provides additional insight into the morphology of complex multi-scale structures [12]. The power-law slopes as well as the critical scattering vector associated with the crossover regime for the lowest LC concentrations are summarized in Fig. 7. The crossover regime decrease as LC content increases, consistent with larger structures dominating the scattering. For the higher LC concentrations, the power-law behavior is consistent with scattering entities exhibiting a mass fractal dimensionality on the 5–80 nm length scale. This corresponds to a percolation cluster or a diffusion-limited aggregate (i.e. lightly branched snowflake structure) and is consistent with the micrographs.

4. Discussion

Photo-induced phase separation (PIPS) processes are analogous to thermally induced phase separation in two-component systems with an upper critical solution temperature (USCT) [1]. In contrast to thermally induced phase separation [13] in which an initially homogenous solution is thermally quenched into the two-phase (either nucleation and growth or spinodal decomposition) regime, reaction-induced phase separation is isothermal. Differences in the final morphology occur due to the rate in which the molecular weight of the polymer increases, essentially moving

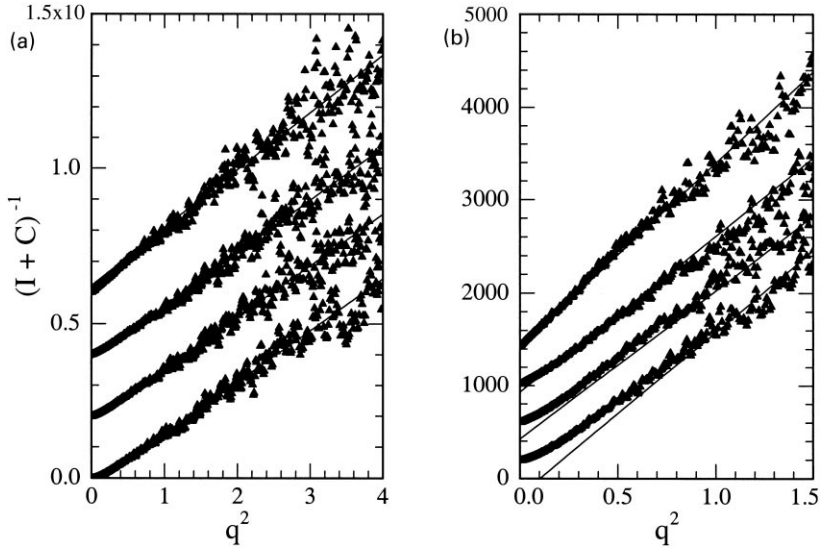

Fig. 8. Zimm plots ($1/I$ vs. q^2) for the low LC composition samples. (a) Data over all q range; (b) data over the low q region. The scattering curves in decreasing order refer to 15, 20, 25, and 35% LC, respectively.

the binodal and spinodal through phase space. Thus for a given composition, PIPS results in a trajectory from one-phase to two-phase regimes comparable to a thermal-quench. For free-radical reactions, a high molecular weight polymer is formed almost instantaneously, equivalent to a rapid thermal quench and spinodal decomposition, irrespective of the initial blend composition. Thus, comparable issues associated with highly non-equilibrium processes, such as meta-stable and/or dynamically frustrated structures and morphologies, are suspected [14]. Furthermore, the high functionality of a penta-acrylate monomer will result in rapid establishment of highly crosslinked regions, which should rapidly aggregate to form a macroscopic gel [15,16]. The subsequent influence on mobilities and mass transport as well as network elasticity restraining formation of phase separated domains all depend critically on monomer concentration. Thus drastic changes in morphology are anticipated and must be understood to optimize PDLC performance.

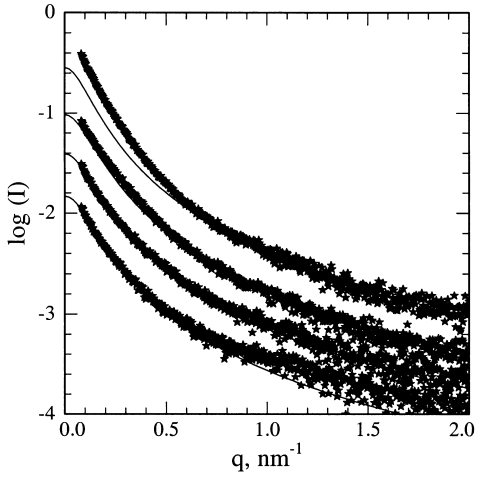

Fig. 9. A comparison of the Ornstein–Zernicke model and the data for samples with less than 25% LC. Line corresponds to the model fit and the points refer to actual data. The scattering curves in increasing order refer to 10, 15, 20, and 25% LC, respectively.

Examination of the SAXS and HRSEM data as a whole indicates that three regions can be defined: (a) $X_{LC} < \backsim 0.20$; (b) $\backsim 0.25 < X_{LC} < \backsim 0.35$; and $\backsim 0.40 < X_{LC}$.

For $X_{LC} < \sim 0.20$, little to no discrete phase separation occurs but scattering length fluctuations exist resulting in finite small-angle scattering. These observations are consistent with a metastable structure arising from density fluctuations of a multi-component system prior to spinodal decomposition, frozen by the rapid cross-linking of the polymer network which elastically inhibits formation of a discrete co-continuous morphology or droplets. The absence of scattering in the pure penta-acrylate indicates that composition fluctuations associated with highly functional monomer and dense network formation are not observable via X-ray diffraction. Furthermore, absence of scattering in the unpolymerized syrups indicates that the initial system is removed from the binodal curve into the one-phase region. As the molecular weight of the polymer increases and the system is rapidly quenched into the spinodal region, density fluctuations precede complete phase separation. Rapid cross-linking of a dense network before phase separation, associated with the high concentration of penta-acrylate monomer, results in a frozen replica of these density fluctuations.

According to classic mean-field theory, the structure

Table 1
Fitting parameters for the Orstein–Zernicke (<25%) and two-component Debye–Bueche (>25%) models

X_{LC}	ξ, (nm)	$I_{OZ}(0)$	a_1, (nm)	a_2, (nm)	f
0.10	7.2(0.05)	0.015(0.001)			
0.15	7.3(0.05)	0.025(0.001)			
0.20	7.5(0.08)	0.038(0.001)			
0.25	8.2(0.2)	0.045(0.003)	3.5(0.2)	21(0.5)	0.98(0.02)
0.35			5.6(0.1)	28(0.5)	0.94(0.01)
0.40			6.2(0.1)	29(0.5)	0.92(0.01)
0.45			6.2(0.1)	28(0.5)	0.91(0.01)
0.50			6.7(0.1)	32(0.5)	0.88(0.01)

factor of concentration fluctuations at small wave vectors is given by the Ornstein–Zernicke [17] Lorentzian function:

$$S_{OZ}(q) = \frac{S_{OZ}(0)}{1 + q^2\xi^2} \quad \text{for } q\xi \ll 1 \tag{2}$$

$S_{OZ}(O)$ is the extrapolated structure factor at $q = 0$ and ξ is the correlation length of the concentration fluctuations. For small volume fraction of scatters where interference effects are minimal, $S(q)$ is directly proportional to $I(q)$. In general, this functional form describes scattered intensity that arises from density fluctuations that exhibit a normal distribution described by the correlation function [11]: $\gamma(r) = 1/r \exp(-r/\xi)$.

Fig. 8 shows the corresponding Zimm plots for small-angle scattering data from 15, 20, 25 and 35% LC. Eq. (2) provides an excellent description of the scattering for compositions equal to or less than 20% LC. Fig. 9 compares the model and observed scattering behavior for $X_{LC} < 0.25$. Substantial deviations from linear behavior occur at the lowest scattering vectors ($q < 0.6\ \text{nm}^{-1}$) for LC concentrations greater than 25%. The excess scattering in the low-q regime is nominally attributed to aggregates and large length scale structures, which is consistent with microscopic observations in this concentration regime. The correlation length and proportionality factors derived from linear-least-squares fit to I^{-1} vs. q^2 and nonlinear-least-square fits to I vs. q are summarized in Table 1. For comparison, the average length (extended) of the five arms originating from the central carbon atom of the penta-acrylate is 0.96 nm. The correlation length of the heterogenieties obtained from the Zimm plots is much larger, and thus does not arise from the fundamental structure of the cross-linked polymer. Additionally, Porod-like scattering for these compositions, if observable, is not anticipated at larger scattering vectors.

According to density fluctuation theories, the square of the correlation length (the wavelength of composition fluctuations in a two-component systems) is proportional to the effective range of intermolecular interactions (Flory's χ parameter) and to the inverse of the gradient of chemical potential with composition. Furthermore, it can be shown that the correlation length depends inversely on 'distance' (in the case of thermal quench, temperature difference) from the critical point. Therefore, ξ is expected to increase as the concentration of penta-acrylate decreases since the system will take longer to form a dense network, effectively approaching closer to the binodal before cross-linking and network elasticity inhibits further mass transfer. Additionally, increases in the LC concentration will decrease the gradient of chemical potential with composition and also result in an increase in the correlation length. A slight increase in ξ is observed in the penta-acrylate/LC system, at $X_{LC} < 0.25$ (Table 1). Additionally, the intercept, $I_{OZ}(0)$, which is proportional to $S_{OZ}(0)$, the product of the volume fraction of the constituents and scattering contrast, should increase, as observed, with volume fraction of LC. Finally, these fluctuations in compositional density will result in a spatially varying cross-link density causing mechanical strength differences spatially throughout the film. This is reflected in the rough, non-glassy fracture surfaces of these samples. The size of the features on the rough fracture surfaces is the same order of magnitude as the wavelength of the compositional fluctuations determined from the SAXS data.

In contrast to the lower LC region, discrete phase separation is observed for $X_{LC} > 0.25$. Here the form of the scattering behavior also changes with LC concentration. Higher LC content and associated decreases in penta-acrylate reduce the cross-link density of the network, enabling the phase separation process to proceed to discrete domains. Increased interfacial tension disrupts the continuity of the density fluctuations, leading to formation of discrete droplets before elasticity of the network constrains additional structural coarsening. The excess scattering at low q is associated with these discrete two-phase structures.

Quantitative analysis of featureless scattering from hierarchical morphologies, such as observed in the micrographs, is complicated by interference between scattering entities as well as polydispersity in size and shape. As such, quantitative analysis of the scattering behavior is extremely model-dependent. Previous studies of inhomogeneous materials, particulate dispersions, porous materials and two-phase blends indicate that a two component Debye–Bueche formulae provides an adequate quantitative description of the scattering [18–20]. Assuming the short and long-range structures are uncorrelated, the general morphology model is described by the weighted sum of correlation functions [21]:

$$\gamma(r) = f \exp(-r/a_1) + (1 - f) \exp(-r/a_2)^2 \tag{3}$$

The two correlation lengths, a_1 and a_2, describe the short and long range fluctuations in scattering power. The fractional contribution for the two structural motifs is f. Physically the two-component model describes a random two-phase structure at small length scales and aggregation at higher length scales. The corresponding scattered intensity

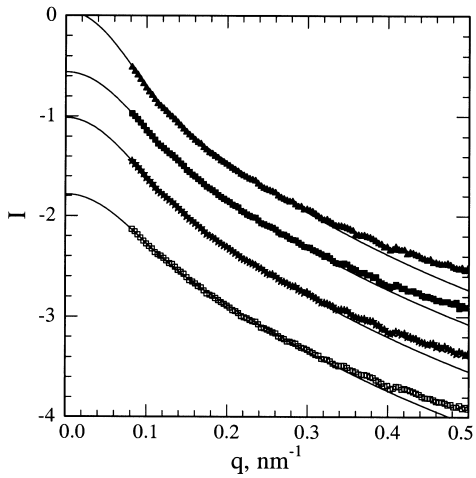

Fig. 10. Two-component Debye–Bueche fit (line) of the data (points) for the high LC concentrations at low q. the scattering curves in increasing order refer to 35, 40, 45, and 50% LC, respectively.

has the form:

$$I(q) = I(0)\left[\frac{2fa_1^3}{(1+q^2a_1^2)^2} + \frac{(1-f)\pi^{1/2}a_2^3}{4}\exp\left(\frac{-q^2a_2^2}{4}\right)\right] \quad (4)$$

Fig. 10 shows the quality of Eq. (3) in describing the low-q scattering data for $X_{LC} > 0.20$. The data is depicted on a semi-log scale to emphasize the decreasing quality of the fit at intermediate q ($q = 0.3$ nm^{-1}) associated with the strong q-dependence of Eq. (3) arising from the assumption of finite interface and Porod-like high-q behavior. The Gaussian contribution to the scattering (exponential term) is necessary to describe the scattering behavior at the lowest q. The resulting three parameters, f, a_1 and a_2, were derived from a four-parameter nonlinear-least-square fit to the data and are summarized in Table 1. Note that it is also possible to assume an Ornstein–Zernicke correlation function for the short-range order. As shown in Figs. 8 and 9, the fits are adequate in the high q scattering regime. However, the low q($<$0.3) data can not be fit by only a Gaussian function as demonstrated below and thus an alternative correlation function was employed.

As X_{LC} increases, the driving force for phase separation increases (larger volume fraction of LC) and the elasticity of the network decreases (lower cross-link density). The Debye–Bueche analysis indicates the presence of 3–7 nm random fluctuations and 20–30 nm aggregates. Note that the value of a_1 is comparable to ξ determined from the Ornstein–Zernicke model, implying the morphological origin of this scatter is similar. Because the parameters are derived from different models and different portions of reciprocal space, absolute comparison of the magnitudes of these correlation lengths is not feasible. The fraction of Guassian component (a_2, 1-f) to the fit increases substantially with LC content indicating that the concentration of this larger-length scale structure is increasing. This is consistent with the physical picture described by the micrographs of discrete LC domains of 20–30 nm embedded in a polymer matrix.

For $X_{LC} > \sim 0.4$, there is insufficient monomer to fully construct a restrictive matrix and the LC phase further condenses into a continuous phase with increasing size (Table 1). Aggregated polymer beads that precipitate from the reactive mixture and aggregate to form a network upon further reaction characterize this inversion in structure. These beads are formed as high molecular weight polymer is generated almost instantaneously due to the high functionality of the monomer and the free-radical polymerization mechanism. These high molecular weight particles are not soluble in the reactive mixture and phase separate out. Being surface rich in functional units, these particles aggregate together and due to the large volume of non-reactive material present (LC), form a porous open cell structure observed in the micrographs.

The size of the beads increases with LC concentration as does their uniformity indicative of differences in timing of the transition from a reaction-limited to diffusion-limited condition. Reaction-limited morphologies are characterized by dense smooth particles whereas diffusion-limited morphologies typically are less dense [22]. The higher LC concentration mixture allows greater bead mobility at comparable time scales thereby delaying the transition in the growth mechanism. Thus, large and smoother beads are observed for the 50% sample relative to the 40% sample. The downturn in the invariant observed in Fig. 5 is consistent with this increased structural homogeneity indicated in the micrographs. The length scales (a_2) obtained from the Debye–Bueche analysis are relatively constant through this composition range.

5. Conclusions

The SAXS and HRSEM results presented suggest three distinctive regimes can be delineated. Below 20% LC, a network structure forms quickly, freezing in density fluctuations before discrete domains form. A small length scale correlation length can be obtained from the SAXS data using the Ornstein–Zernicke model. These density fluctuations manifest themselves as fracture surface features due to spatial heterogeneity in the film structure. Between 20 and 35% LC, small discrete domains of LC can be observed. As the amount of monomer decreases, the network elasticity decreases. We speculate that it has decreased to a point where interfacial tension breaks up the spinodally driven fluctuations into discrete domains. The SAXS data can be modeled using a two component Debye–Bueche model which yields short range fluctuations comparable to the Ornstein–Zernicke model as well as a long-range correlation lengths commensurate with the domain sizes observed with HRSEM. Above 35% LC, an inversion in the

morphology occurs where the LC phase becomes continuous. Because of the large composition of non-reactive components, polymerization of the monomer results in the formation of small polymer beads, which are insoluble and phase separate out. As composition is increased, the structural homogeneity of the two-phase morphology increases, which is consistent with a downturn in the invariant data.

The use of SAXS has been demonstrated to be a powerful tool in examining the development of two-phase structure in PDLC composites. Although HRSEM and SAXS probe at different length scales, the data obtained by both is complementary. The wealth of information obtained by SAXS techniques, particularly in the low LC concentrations where phase separation occurs but cannot be observed using HRSEM (and other techniques), is important in understanding the fundamental physics associated with structure development. This work indicates that real-time monitoring of the structure development, using SAXS while curing, would be beneficial to better understand the structure development in these materials.

References

[1] Drzaic PS. Liquid crystal dispersions. Singapore: World Scientific, 1995.
[2] Chigrinov VG. Liquid crystal devices. Boston: Artech House, 1999.
[3] Sutherland RL, Tondiglia VP, Natarajan LV, Bunning TJ. Chem Mater 1993;5:1533.
[4] Tanaka K, Kato K, Tsuru S, Sakai S. J SID 1994;2:37.
[5] Crawford GP, Fiske TG, Silverstein LD. SID Int Symp Dig Tech Papers, vol. 27, 1996. p. 99.
[6] Pogue RT, Sutherland RL, Schmitt MG, Natarajan LV, Siwecki SA, Tondiglia VP, Bunning TJ. Appl Spectrosc 2000;54:1.
[7] Bunning TJ, Natarajan LV, Tondiglia VP, Sutherland RL. Annu Rev Mater Sci 2000;30:83.
[8] Odian G. Principles of polymerization. New York: Wiley, 1981.
[9] Bunning TJ, Natarajan LV, Tondiglia VP, Sutherland RL, Vezie DL, Adams WW. Polymer 1995;36:2699.
[10] Rapp G, Gabriel A, Dosiere M, Kock MHJ. Nucl Instrum Methods Phys Res, Sect A 1995;357:178.
[11] Glatter O, Kratky O. Small angle X-ray scattering. New York: Academic Press, 1982.
[12] Schmidt PW. In: Avnir D, editor. Fractal approach to heterogeneous chemistry. New York: Wiley, 1998. p. 67.
[13] Olabisi O, Robeson LM, Shaw MT. Polymer–polymer miscibility. New York: Academic Press, 1979.
[14] Tran-Cong Q, Kawai J, Endoh K. Chaos 1999;9:298.
[15] Serbutoviez C, Kloosterboer JG, Boots HMJ, Touwslager FJ. Macromolecules 1996;29:7690.
[16] Bunning TJ, Natarajan LV, Tondiglia VP, Dougherty G, Sutherland RL. J Polym Sci, Part B 1997;35:2825.
[17] Liao G, Xie Y, Ludwig KF, Bansil R, Gallagher P. Phys Rev E 1999;60(4):4473.
[18] Fernandez AM, Wignall GD, Sperlling LH. Adv Chem 1986;211:10.
[19] Longmon GW, Wignall GD, Hemminh H, Dawkins JV. Colloid Polym Sci 1974;252:298.
[20] Wignall GD, Farrar NR, Morris S. J Mater Sci 1990;25:69.
[21] Moritani M, Inoue I, Molegi M, Kawai H. Macromolecules 1970;33:433.
[22] Rajaram CV, Hudson SD, Chien LC. Chem Mater 1996;8:2451.